Geothermal Energy

RESEARCH Open Access

A probabilistic model-based approach to assess and minimize scaling in geothermal plants

Pejman Shoeibi Omrani[1,2*], Jonah Poort[2], Eduardo G. D. Barros[3], Hidde de Zwart[2,4], Cintia Gonçalves Machado[3], Laura Wasch[3], Aris Twerda[2], Huub H. M. Rijnaarts[1,5] and Shahab Shariat Torbaghan[1]

*Correspondence:
pejman.shoeibiomrani@tno.nl

[1] Environmental Technology, Wageningen University & Research, Bornse Weilanden, Wageningen, The Netherlands
[2] Heat Transfer and Fluid Dynamics, TNO, Kessler Park 1, Rijswijk, The Netherlands
[3] Applied Geosciences, TNO, Princetonlaan, Utrecht, The Netherlands
[4] Mechanical Engineering, TU Delft, Mekelweg, Delft, The Netherlands
[5] Institute for Circular Society of the EWUU Alliance, Universities of Eindhoven, Wageningen, Utrecht and University Medical Centre Utrecht, Utrecht, The Netherlands

Abstract

Geothermal installations often face operational challenges related to scaling which can lead to loss in production, downtime, and an increase in operational costs. To accurately assess and minimize the risks associated with scaling, it is crucial to understand the interplay between geothermal brine composition, operating conditions, and pipe materials. The accuracy of scaling predictive models can be impacted by uncertainties in the brine composition, stemming from sub-optimal sampling of geothermal fluid, inhibitor addition, or measurement imprecision. These uncertainties can be further increased for fluid at extreme conditions especially high salinity and temperature. This paper describes a comprehensive method to determine operational control strategies to minimize the scaling considering brine composition uncertainties. The proposed modelling framework to demonstrate the optimization under uncertainty workflow consists of a multiphase flow solver coupled with a geochemistry model and an uncertainty quantification workflow to locally estimate the probability of precipitation potential, including its impact on the hydraulic efficiency of the geothermal plant by increasing the roughness and/or decreasing the diameter of the casings and pipelines. For plant operation optimization, a robust control problem is formulated with scenarios which are generated based on uncertainties in brine composition using an exhaustive search method. The modelling and optimization workflow was demonstrated in a geothermal case study dealing with barite and celestite scaling in a heat exchanger. The results showed the additional insights in the potential impact of brine composition uncertainties (aleatoric uncertainties) in scaling potential and precipitation location. Comparing the outcome of optimization problem for the deterministic and fluid composition uncertainties, a change of up to 2.5% in the temperature control settings was observed to achieve the optimal coefficient of performance.

Keywords: Uncertainty quantification, Robust optimization, Scaling, Precipitation, Geothermal production

Introduction

In geothermal operations, mineral precipitation is a common problem that occurs when geothermal saline water (brine) is extracted from underground reservoirs and brought to the surface for the thermal energy production. The hot brine typically contains high concentrations of dissolved minerals, which can precipitate out of the solution due to the changes in the temperature and pressure during its transport from the production to the injection wells. Multiple geothermal sites around the globe are currently facing scaling issues (Ramsak 2015; Heuvel et al. 2018). Numerous studies (Boersma et al. 2018; Grassinani 2000) analyzed different precipitated minerals observed in geothermal systems such as barite, celestite and galena deposits which were found to have a significant impact on the performance of the geothermal sites.

The scaling is strongly related to geological conditions, wellbore materials, fluid flow properties, and operational conditions (Regenspurg et al. 2015). Scaling can lead to several processes that reduce system efficiency, including heat exchangers fouling and pipeline blockage. The fouling of heat exchangers is one of the common problems caused by scaling in geothermal operations. These deposits can reduce the heat transfer efficiency of heat exchangers by creating an insulation layer, resulting in lower energy production, higher operating costs, and a lower coefficient of performance (COP) (Led´esert et al. 2021). To mitigate the problem of scaling, various approaches have been developed, including chemical treatments, mechanical cleaning, and thermal treatments. Chemical treatments involve the use of chemical inhibitors to prevent mineral precipitation, deposition, or dissolve existing deposits (Pauwels et al. 2022). Mechanical cleaning involves physically removing the deposits from the heat exchanger surface using brushes, high-pressure water, or other cleaning methods.

Next to the treatments mentioned above, controlling the process conditions in geothermal plants could have an impact on the initiation or rate of scaling in the system. Such operational decisions need to be made fast (in operational time-scales) and operators frequently require support to make informed decisions (Raos et al. 2022). Several models and methods were developed to quantify the risk of scaling in geothermal plants which can be used to identify optimal control settings of the system (Wasch et al. 2019). A reliable prediction of scaling potential and its impact on the production behavior relies significantly on three key factors: (1) the characterization of the geothermal fluid, a process influenced by uncertainties stemming from fluid sampling and analysis, (2) the interplay between flow hydrodynamics and deposition caused by scaling and (3) a reliable geochemistry modelling of the geothermal fluid. The fluid compositions are evaluated through sampling of the geothermal fluid and laboratory analysis and all these steps are impacted by uncertainties, depending on, e.g., location of fluid sampling, uncertainties in test conditions and procedures, such as sample preservation and container cleaning (Ármannsson and Ólafsson, 2007). Especially for geothermal fluids under extreme conditions, which are defined as fluid temperatures > 100 °C and up to critical conditions and/or salinity > 35 g/l, the physical and chemical properties are poorly defined and this causes additional errors and uncertainties in the prediction and control of flow-chemistry processes in geothermal plants (Kieling et al. 2023).

Most of the current studies to estimate the scaling risks in geothermal systems and assessing the impact of operational settings on scaling are performed by analyzing the

scaling potential at different process conditions with a focus on a reliable geochemistry modelling of the geothermal fluid (Bozau et al. 2015; Andre et al. 2019; Shabani et al. 2020). So far, the impact of fluid composition uncertainties on the operational strategies of geothermal plants have not been studied. Such an approach will require a modelling framework that can couple the geochemistry with the production behavior in the geothermal plants and an optimization framework that can deal with uncertainties. The primary objective of this study was to formulate a robust decision support workflow for uncertainty quantification in geothermal operation to monitor, forecast, and minimize the scaling in geothermal plants considering fluid composition uncertainties, which can be more challenging for geothermal fluid under extreme conditions.

First, a fluid production model that accounts for uncertainties in the physico-chemical properties of the geothermal fluid is developed. The developed methodology encompasses a two-way coupling between scale deposition and flow attributes. This implies that minerals precipitating and depositing on equipment surfaces subsequently impact flow rates within the system (by altering the tubing diameter and roughness), as well as temperatures (by reducing heat transfer efficiency) and pressures. Second, the developed model was coupled to an uncertainty quantification method to propagate the aleatoric uncertainties (Mariotti et al. 2016) in fluid composition to the developed flow-chemistry model to estimate the uncertainty in the scaling potential resulted from fluid composition uncertainties. Finally, an optimization problem is formalized as a scenario based deterministic optimization to support the operation strategy to minimize scaling in a geothermal plant. All the steps were applied to a hypothetical case study of a low-enthalpy geothermal plant suffering from celestite and barite precipitation in the heat exchanger.

The main scope of the study was on the development of a decision support workflow for operational strategies under uncertainties and not a fully validated modelling framework. It is important to note that the choice of the geochemical and fluid dynamics models and their parameters, known as model or epistemic uncertainty, will also have a major impact on the uncertainties of the scaling estimation (Hörbrand et al. 2018) and production forecasting. This topic was not in the scope of the paper due to the lack of experimental and measurement data and the employed models were selected solely for the demonstration of the optimization workflow. To the best of the authors' knowledge, this paper introduces a novel modelling and optimization under uncertainty workflow tailored to enhance the operational efficiency of geothermal plants and mitigate unwanted scaling within the system. In addition, this work addresses a unique integration of hydrodynamic and scaling within geothermal plant modeling.

Methodology

Hydraulic–chemistry model

Figure 1 provides a schematic of the workflow of the coupled flow and chemistry model. The workflow initiation involves defining system geometry, including parameters, such as pipe lengths, diameters, materials, and boundary conditions. These inputs will be used to setup the hydraulic model, which in this case a 1-D drift–flux multiphase flow model is employed based on an existing solver developed in-house. The drift–flux model accounts for the relative velocity (known as drift velocity) between the phases, to support the

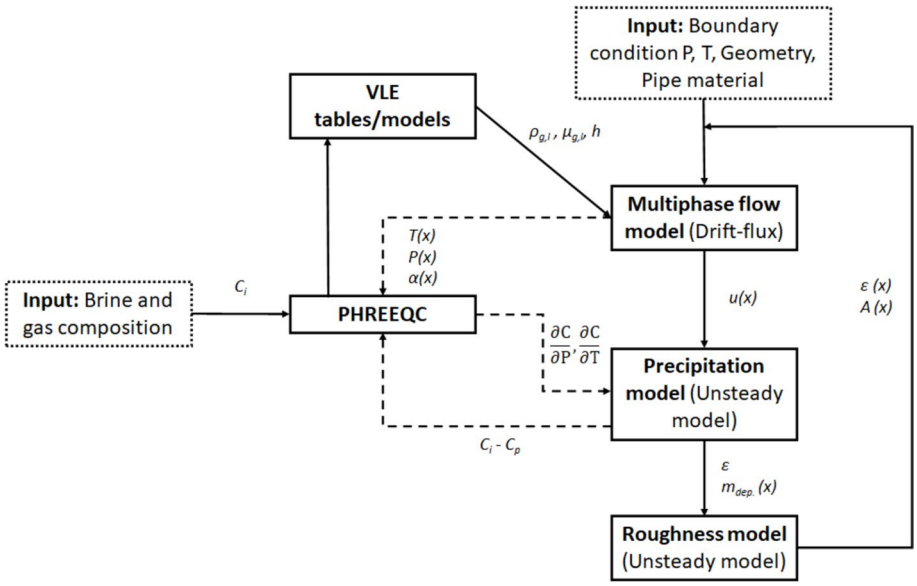

Fig. 1 Hydraulic–chemistry modelling framework integrating multiple solvers and models to calculate the hydrodynamics of the flow, precipitation chemistry and accumulation of precipitation leading to a modification of roughness

prediction of phase distribution and average velocities in the multiphase fluid flow. By considering the multiphase flow inside the pipes, the 1-D formulation of the Navier–Stokes equation will be

$$\frac{dP}{dx} = \left(g\sin(\theta) + \frac{f}{2D}|u_m|u_m\right)\left(\alpha_g\rho_g + \alpha_l\rho_l\right) - \alpha_g\rho_g u_g\frac{du_g}{dx} - \alpha_l\rho_l u_l\frac{du_l}{dx},$$

$$u_m = \alpha_g u_g + \alpha_l u_l$$

in which P is the pressure, g is gravitational acceleration, θ is the inclination of the pipe, D is the diameter of the pipe, and f is the Fanning friction coefficient. In the formulation, the hold-up is denoted as α, density as ρ and superficial velocity as u, with the subscripts g and l stands for gas and liquid phase. The mixture velocity, u_m, is given as the sum of the gas and liquid superficial velocities. In multiphase flow, there could be a difference between the gas and liquid velocity which is caused by the slip between the phases. We used the drift–flux model to account for the slip between the gas and liquid phase (in case of solid phase present, the solid phase is assumed to be present as a mixture in the liquid):

$$u_g = C_0 u_m + u_d$$

where C_0 is the distribution parameter (assumed to be 1.2) and u_d is the drift velocity of the gas derived as (σ is the surface tension):

$$u_d = 1.53\left[\frac{\sigma g\left(\rho_l - \rho_g\right)}{\rho_l^2}\right]^{1/4}$$

The solver is steady-state at each point in time (time-step) and it will calculate all the required flow properties, such as flow rates, velocities, local pressures, and temperatures. The model is divided into 1-D computational cells. For the selected case study, which is the scaling in a heat exchanger, since the heat exchangers in geothermal plants are installed downstream of a gas–liquid separator or degasser, no-slip between liquid and gas phase is calculated in the model. However, for other case studies in the future, e.g., flow in the wellbore or pumps, the higher slip velocity is expected depending on the flow regimes. For both fluid properties and potential scaling, the composition of the geothermal brine and gas must be included. The composition is fed into a geo-chemical speciation solver, PHREEQC (Parkhurst et al. 1999) which can calculate both fluid properties and precipitated amounts at each computational cell. Precipitation is modelled up to equilibrium, without considering remaining supersaturation due to kinetic inhibition by the slow reaction rates. As such the modelled precipitation relates to maximum potential scaling.

The hydraulic model requires fluid properties, such as density and viscosity, at different pressure, temperature (PT) conditions to solve the resulting flow rate in the system. The fluid properties are provided by the vapor–liquid equilibrium (VLE) table or models linked to the drift–flux model. In case of availability of other models or libraries for VLE table, those can be directly integrated in the drift–flux model but in this framework the fluid properties are calculated for a range of PT conditions and then fed into a VLE table to be used by the drift–flux model. The drift–flux model solves the fluid flow properties and output the flow properties and phase velocities (or flow rates) to the precipitation model. The PHREEQC will provide potential scaling to the roughness model based on the resulting temperature, pressure, and phase fraction from the multiphase flow model. The resulting precipitation will be translated to an effective roughness (using the roughness model block) and the new roughness is fed back to the drift–flux model to calculate the flow properties and scaling in the next time step.

In this framework, a two-way coupling modeling workflow was developed meaning that the impact of flow and process conditions on the amount of scaling is calculated and as a result of the maximum potential precipitation, the flow properties will be modified in the next time steps. Upon determining precipitation quantities per cell, the deposition and roughness models (impacted by deposition) assess the impact of newly formed scale layers on inner diameter, roughness, and heat transfer of the pipe. Updated values are then applied in the next time-step to adjust the flow, pressure, and temperature, leading to subsequent changes in precipitation and pipe properties. This iterative process will continue until the production behavior forecasting is performed in the desired time horizon.

Two-way coupling of flow and precipitation interaction

As described in the modelling workflow, the amount of precipitation will be calculated using PHREEQC model, which needs to be converted into a deposition profile. This is done through the developed roughness model. For this model, the mineral precipitation quantity per cell is the main input parameter. As the output of the mineral precipitation is in mol/L, the volumetric deposition of each mineral at a given cell is calculated as follows:

$$V_{cell} = Dep_{cell}.Q_{brine}.\frac{Molarmass}{\rho_{mineral}}.\Delta t.1000$$

in which.

V_{cell}: Volumetric mineral deposition per cell (m^3).

Dep_{cell}: Expected mineral deposition from PHREEQC (mol/L).

Q_{brine}: Volumetric flow rate of the geothermal brine (m^3/s).

Molar mass: Molar mass of the concerned mineral (kg/mol).

$\rho_{mineral}$: Mineral density (kg/m^3).

Δt: Time period after which the scaling model is updated (s).

The shape of the precipitated minerals will depend on the type of mineral and surface properties. In earlier studies, it was found that for the type of scaling in low enthalpy geothermal systems, it is energetically favorable to attach to the pipe walls (metal walls) as opposed to being clustered together (Boersma et al. 2018). This is due to adsorption of positively charged ions from the bulk flow to the negatively charged pipe wall. Therefore, the crystals will preferentially start to cover the pipe wall before they accumulate and cluster together. The precipitated mineral shape is also driven by the mineral surface energy and flow properties. As this study focuses on barite and celestite precipitation, it was found that they, similar to galena, will precipitate in a conical shape under turbulent flow conditions (Moriconi et al. 2022). In this work, it is assumed that deposition growth over time will not change the shape of the deposited layer and instead it accumulates radially towards the center of the tubing. The volumetric deposition at each cell is assumed to be uniformly distributed (Fig. 2). Solving for the deposition thickness:

$$\delta_{dep,i} = R - \sqrt{R^2 - \frac{V_{dep,i} - V_{dep,1}}{\pi.L_{cell}}}$$

where.

$\delta_{dep,i}$: Deposition thickness at a given cell after i^{th} time iteration [m].

R: Radius of the pipe [m].

$V_{dep,i}$: Total volumetric mineral deposition after i^{th} time iteration [m^3].

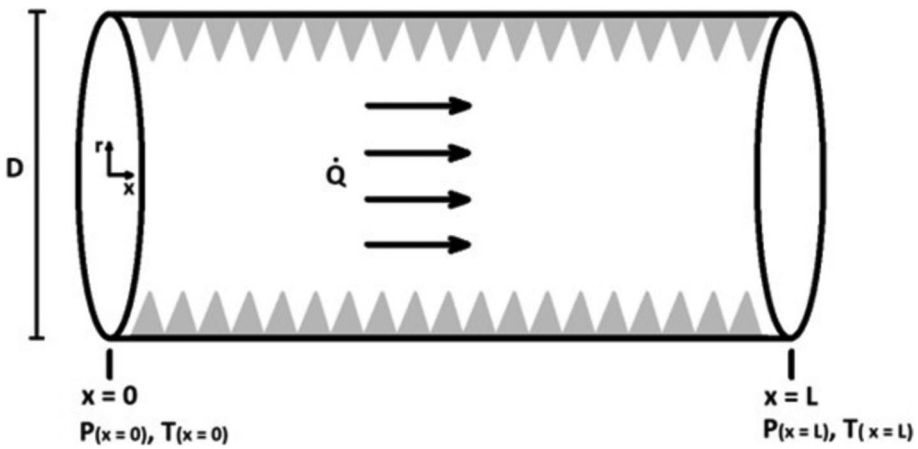

Fig. 2 Impression of the deposition profile distribution in a single computational cell

$V_{dep,1}$: Total volumetric mineral deposition after the initial time iteration [m^3].

L_{cell}: Length of the computational cell [m].

As the deposition thickness grows radially towards the center of the tubing, the hydrodynamics of the flow will be impacted. Additional pressure drop induced by mineral deposition is evaluated considering both the change in the surface roughness and the reduction in the effective flow area. The pressure drop associated with the surface roughness can be determined by solving the Darcy–Weisbach equation (Kudela 2009):

$$\Delta P_{roughness,cell} = \frac{f.L_{cell}}{R - \delta_{dep,cell}}.\rho u_m^2$$

in which.

$\Delta P_{roughness,\,cell}$: Pressure drop in a grid cell [kg/(m^2.s)].

f: Fanning friction factor [-].

ρ: Liquid density [kg/m^3].

u_m: Mixture velocity [m/s].

For calculating friction coefficient, the mean deposition height is estimated by averaging the deposition height profile along a grid cell. The equivalent surface roughness is derived as (Willmott et al. 2006):

$$\epsilon_{cell} = \sqrt{\frac{1}{n}\sum_{n}\left(H_{dep,cell} - \overline{H_{dep,cell}}\right)^2}$$

where.

ϵ_{cell}: Surface roughness in each cell [m].

n: Considered number of discrete samples per cell.

$H_{dep,cell}$: Height of the deposition profile varying with n [m].

$\overline{H_{dep,cell}}$: Mean height of the deposition profile per cell [m].

Coefficient of performance estimation

The coefficient of performance (COP) is a measure of the efficiency of a heating, cooling, or refrigeration systems. It is defined as the ratio of the desired output of the system (in this case heating) to the required input (energy consumption or work done) to achieve that system output:

$$COP = \frac{Q_{transfer}}{W_{ESP}}$$

where $Q_{transfer}$ is the energy extracted from the geothermal system in the heat exchanger, and W_{ESP} is the power consumed by the electrical submersible pump (ESP), given by

$$Q_{transfer} = \sum_{cell}\frac{\delta T}{R_{thermal,cell}}$$

$$W_{ESP} = \frac{Q_{volumetric}}{3600.\eta_{ESP}}\left(\rho_{brine}.g.h_{hydro,head}\right)$$

With δT being the temperature difference between geothermal fluid and working fluid of the heat exchanger, η_{ESP} is the ESP efficiency and $h_{hydro,head}$ is the hydraulic head of the ESP to supply the desired flow rate ($Q_{volumetric}$), calculated based on an example pump curve. The produced heat is calculated based on the heat transfer in the heat exchanger, taking into account the conduction heat transfer in the pipe tubing and scaling layer and the heat convection in the brine flow inside the tubing and convection outside the tubing. The convection heat transfer is derived based on Gnielinski's formulation (Gnielinski 1975), defined as follows:

$$R_{thermal} = \frac{1}{2\pi L_{cell}} \left(\frac{1}{(r_{ID} - \delta_{dep,cell}).h_{conv,in}} + \frac{ln\frac{r_{ID}}{r_{ID}-\delta_{dep,cell}}}{k_{scaling}} + \frac{ln\frac{r_{OD}}{r_{ID}}}{k_{tubing}} + \frac{1}{r_{OD}.h_{conv,in}} \right)$$

$$Nu = \frac{h_{conv,in}D}{k_{fluid}} = \frac{\frac{f}{8}(Re - 1000)Pr}{1 + 12.7(\frac{f}{8})^{0.5}(Pr^{2/3} - 1)}$$

in which Nu is the Nusselt number, Pr is Prandtl number, and Re is Reynolds number. Heat conduction of both tubing (k_{tubing}) material and scaling ($k_{scaling}$) are also included in the thermal resistance calculation. Nusselt number is used to calculate the convection heat transfer coefficient (h_{conv}) using the pipe diameter and the thermal conductivity of the fluid (k_{fluid}). Note that COP depends on the temperature and pressure in the heat exchanger, and on the volumetric flow rate, since these parameters will impact the scaling behaviour. As the forward model, the multiphase flow solver coupled with PHREEQC showed in the previous section was used to calculate the COP under different operation conditions.

Uncertainty quantification (UQ)

Uncertainty quantification (UQ) is a systemic approach to modelling that aims to characterize the impact of different uncertainty sources on the outcome of a model (Zhang 2020). In the scaling modelling approach described in this work, uncertainty mainly arises from two factors: epistemic uncertainties, known as model uncertainties and aleatoric uncertainties, known as uncertainties in input parameters. The focus of the UQ analyses done in this work was on the latter of these two sources, more specifically on the uncertainty in scaling calculated by the models arising from uncertainties in the brine composition. Uncertainties related to differences between available thermodynamic databases are substantial in geochemical modelling, especially given to the high salinity of geothermal fluids. This uncertainty is, however, not taken into account, and we assume that for an actual case, a thermodynamic database would be selected that is most suitable for the composition and conditions of the brine which can be part of future work.

In this study, Monte Carlo sampling was employed to assess the uncertainty associated with scaling potential, influenced by uncertainties in fluid composition (Zhang 2020). Uncertain parameters with a given or characterized probability distribution are propagated through the model by a random sampling. This process yielded an ensemble of outputs, characterized by their respective probability distributions. Subsequently, statistical analysis was conducted on this output distribution. The analysis

supported the investigation of the impact of each input parameter on the output of the model. The Monte Carlo is schematically depicted in Fig. 3.

Uncertainty quantification can be used to obtain insights into the probability distribution of a model's quantity of interest given a probability distribution on its inputs. In addition, UQ can also be used to investigate the impact of each uncertain parameter on the model predictions using Sobol sensitivity indices (Saltelli et al. 2010). It is a variance-based sensitivity analysis approach, in which the magnitude of the impact of a given input parameter and combination of input parameters on the output is quantified (Saltelli et al. 2010). In Sobol analysis, first-order effects measure the impact of varying a single parameter on the model output, while second-order effects are the ones obtained from varying two parameters to derive the degree of influence of their interaction over the output response. This method offers a global sensitivity analysis, estimating how uncertainty in a model's output can be attributed to different sources of uncertainty in its inputs. Consequently, the conclusions from the sensitivity analysis are highly dependent on the sources and ranges of uncertainty in the input parameters.

To compute the Sobol indices, a specific type of sampling scheme is used, called Sobol sampling. Sobol sampling generates quasi-random samples which are more evenly distributed between the upper and lower bounds of the sampling limits, allowing for more accurate and efficient computing of the Sobol sensitivities (Dwight et al. 2016). For a more in-depth description of the Sobol sampling scheme and exact computation of the Sobol sensitivity indices, the reader is referred to (Saltelli et al. 2010). In this work, the"SALib" package (Herman et al. 2017; Iwanaga et al. 2022) in the Python programming language was used to generate the samples and determine the Sobol indices. The outcome of the Sobol sensitivity analyses was used to determine the uncertainties in which brine ions were most significant in determining the potential amount of scaling. This was used to limit the number of uncertain parameters in the two-way coupled analysis by taking the most significant uncertain ions, allowing for a reduction in the total number of realizations and, thereby, speeding up the modelling and optimization process.

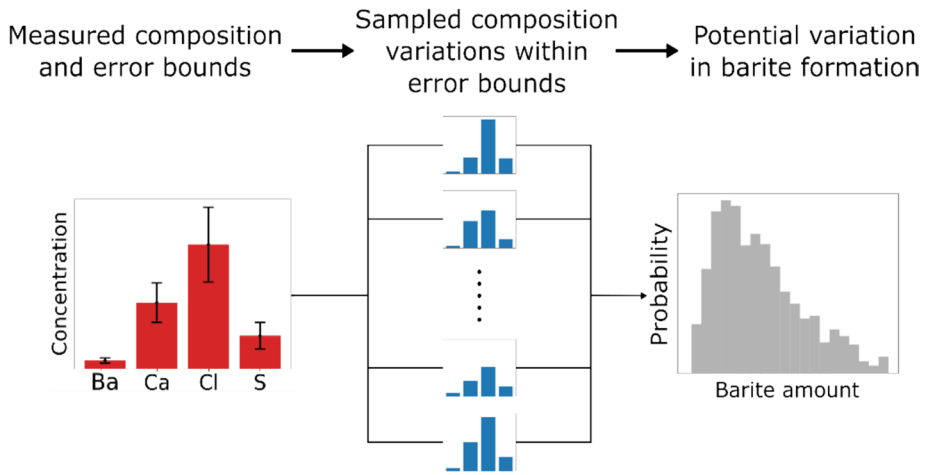

Fig. 3 Schematic diagram of the uncertainty quantification workflow

Robust control problem

In this section, we describe the robust control problem (RCP) solved to determine the optimal operational settings to maximize the geothermal system efficiency while minimizing the negative impact of scaling.

Parametric uncertainty

The solution of the RCP is achieved through a model-based optimization methodology. The first robustness aspect considered here refers to the search for operational strategies that account for input parameter uncertainty throughout the optimization procedure. This means that some input parameters of the simulation models described in previous sections are considered to be uncertain, with values subject to a probability distribution based on the knowledge available at the moment of the assessment. Here we rely on a scenario-based approach to accomplish the quantification of the parametric uncertainty, meaning that, instead of considering a single deterministic base–case model, we utilize an ensemble of model realizations (i.e., a set of model scenarios: instances of the same model, but with different values of the uncertain parameters) to guide the robust optimization. The underlying goal of the optimization is to find the solution that is simultaneously optimal to all the considered scenarios. By accounting for scenarios that sufficiently span the expected degree of uncertainty, the optimized solution obtained with this approach will typically not be the best performing for each scenario individually but will be the one that is statistically the most likely to improve the performance of the ensemble as a whole. In this study we consider the maximization of the expected value of target objective function over the ensemble, which is mathematically formulated as

$$\max_{\mathbf{u}} \bar{J}(\mathbf{u}), \text{with}$$

$$\bar{J}(\mathbf{u}) = \frac{1}{N_\mathrm{r}} \sum_{k=1}^{N_\mathrm{r}} J^k(\mathbf{u}, \mathbf{m}_k),$$

where $\bar{J}(\mathbf{u})$ is the mean of the objective function value being optimized for a single strategy u based on each $J^k(\mathbf{u}, \mathbf{m_k})$ which is the objective function evaluated for each k^{th} model realization m_k and N_r is the number of realizations considered. Note that in this particular formulation, we assume the model realizations to be equiprobable (i.e., equally weighted). However, in case there is knowledge available about the likelihood of each realization, this can be incorporated by introducing weighted averaging with weights proportional to the probabilities expected for each scenario. There exist several numerical methods to solve scenario-based robust optimization problems. These range from perturbation-based stochastic gradient methods with computationally efficient solutions to handle large ensembles of computationally intensive function evaluations (e.g., StoSAG approach proposed by Fonseca et al. 2017) to derivative-free methods for broad exploration of the optimization space at the cost of a larger number of model evaluations (Echeverr´ıa Ciaurri et al. 2011). The particular case considered in this study is relatively simple in terms of the size of the optimization problem, allowing us to solve the optimization by exhaustive search of the entire control variable domain.

Operational flexibility

The second robustness aspect explored in this study concerns the flexibility of the optimized operational settings, specifically the capacity to deviate from the optimal control value without significant compromise in performance. To gain quantitative insight into such operational flexibility, the control problem is modified from a point-based into a range-based optimization problem. Instead of evaluating the performance in terms of the objective function for a single control value u, we seek ranges (or intervals) of control values $[u^l, u^u]$ that deliver the best expected performance. Our approach here is rather straightforward and consists of parametrizing the control ranges to be optimized by a range size Δ_u and the lower bound of the range u^l. The optimizer can then search the optimal range of controls (i.e., defined by lower and upper bound values) for a given range size by evaluating a predefined number of evenly distributed control values within that range size. In mathematical terms, this corresponds to solving:

$$J_r\left(\mathbf{u}^l, \mathbf{m}\right) = \frac{1}{N_\Delta} \sum_{\mathbf{u}\in[\mathbf{u}^l, \mathbf{u}^l+\Delta_\mathbf{u}]} J_v(\mathbf{u}, \mathbf{m}),$$

where J_r is the range average of point-based objective function J_v being optimized for a set of control values u ranging from the lower-bound range value u^l and the upper-bound range value $u^l + \Delta_u$. The average is a simple arithmetic average from the set of controls within the considered range, which size N_Δ (i.e., number of control values) depends on the range size. Note that the range-based optimization workflow is decoupled in two steps by optimizing only the range of a given (fixed) range size, and, after that, repeating the procedure exhaustively for several pre-selected range sizes. In case of optimization problems with a significantly larger number of control variables, an approach would be to formulate the problem as a two-level nested optimization exercise (Bellout et al. 2012), where the range size could be optimized in the outer-loop and the range itself could be optimally selected in the inner-loop of the optimization. The procedure explained above can potentially be combined with the robust scenario-based approach previously described to incorporate the parametric uncertainty. Figure 4 depicts the model-based procedure followed to solve the formulated scenario-based robust optimization problems described above, both for the point-based and range-based variations.

For point-based optimization, as shown in the left flowchart, the process begins with defining model scenarios and optimization variables (including control variables and their bounds). This is followed by an optimization step to evaluate the objective function across all scenarios, ultimately identifying the optimal control point for each realization. For range-based optimization, shown in the right flowchart, the steps are largely similar. However, instead of evaluating a single control point, the objective function is evaluated for all points within the selected range across all scenarios. This approach accounts for variability within the range to identify the optimal solution.

Results

Case study description

Barite and celestite precipitation in the heat exchanger of a geothermal system is selected as a hypothetical case study. The geothermal plant is a low-enthalpy hydro-thermal

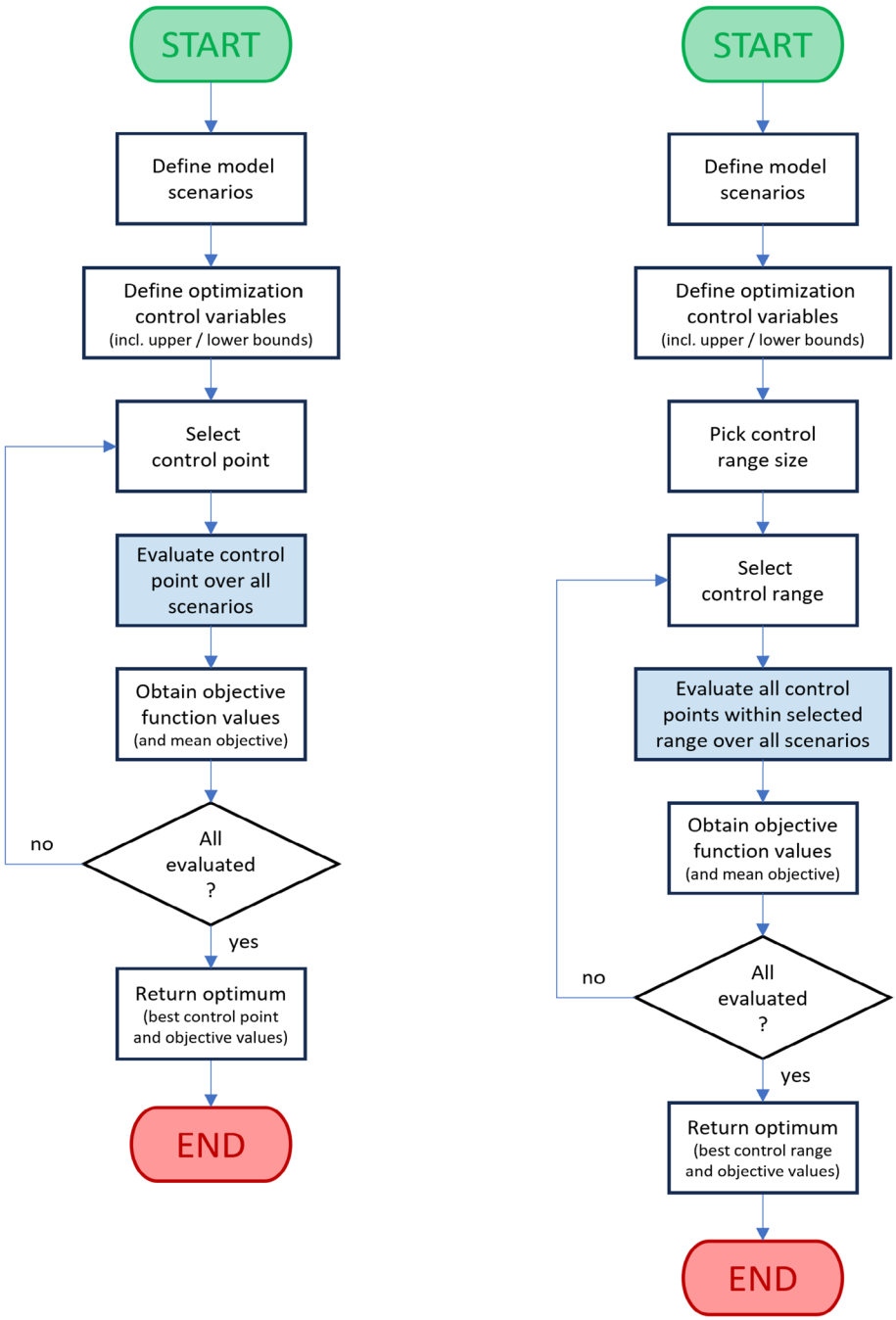

Fig. 4 Optimization workflows to solve the robust control problem (RCP): point-based optimization (left) and range-based optimization (right)

system suited for heating and direct use application. The main components of the geothermal brine and their associated uncertainties are summarized in Table 1. The uncertainty ranges were derived from an earlier study on the REFLECT geothermal fluid database to characterize the uncertainties in fluid elements (Poort et al. 2022). To prevent charge imbalance due to random variations in the anion and cation concentrations, the Cl^- concentration is adjusted for charge balance for every solution composition. The

Table 1 Nominal concentrations and uncertainties of brine elements in the case study, all the uncertainties are treated as a Gaussian distribution

Elements	Concentration [mol/kgw] ([mg/l])	Uncertainties %
Na^+	3.9 (85000)	±2
K^+	$6.2*10^{-2}$ (2200)	±0.5
HCO_3^-	$4.5*10^{-3}$ (0.001)	±3
Ca^{+2}	$2.0*10^{-1}$ (7450)	±3
Mg^{+2}	$5.2*10^{-2}$ (1150)	±4
Ba^{+2}	$4.3*10^{-5}$ (5.5)	±3
Sr^{+2}	$3.6*10^{-3}$ (290)	±2
Fe^{+2}	$3.4*10^{-3}$ (175)	–
Cl^-	4.472 (145000)	±3
SO_4^{-2}	$6.7*10^{-3}$ (585)	±4
Mn^{+2}	$1.8*10^{-4}$ (9.25)	–

The concentration of mg/l is defined at temperature of 21 °C and the nominal concentration leads to the brine density of 1.1682 g/cm^3

model is set up by equilibrating every fluid composition at reservoir conditions (100 °C and 331 bar) as well as with a gas phase. The main components of the gaseous phase dissolved in geothermal brine are CO_2, CH_4 and N_2 and the uncertainties in gas compositions were not considered in this study. The gasses are included as fixed pressure 'GAS_PHASE' in PHREEQC, with CO_2 as the only reactive gas and CH_4 and N_2 modelled as redox-uncoupled. The Pitzer database (pitzer.dat in PHREEQC) was used for the PHREEQC calculations (Pitzer 1973, 1991) due to its ability to handle high ionic strength solutions. Several studies have successfully applied the Pitzer model to brines with high salinities (Christov et al. 2012; Andre et al. 2019). The results of the scaling prediction can be strongly dependent on the choice of the geochemistry model and databases which is not the scope of this manuscript. Thus, the results for the scaling potential should be interpreted with caution, and further validation against experimental data would be beneficial to ensure the model's accuracy under these extreme conditions. Since the compositions at extreme conditions are complex, no general statement can be made on the impact of ion activity models on interactions between brine and minerals.

The PHREEQC calculations were used to achieve predictions of gas partial pressures with temperature and pressure. All gasses are dissolved at reservoir pressure and the dissolution of CO_2 decreases the pH from the initial value of 6.2 to a pH of 4.7 at reservoir conditions. Equilibrium of barite in the reservoir is applied to ensure there is no initial supersaturation for barite and celestite that would yield immediate precipitation upon following model steps. A second model step involves reducing the pressure to 10 bar due to production to the surface, with partial exsolution of gasses (with a pH increase to 4.9 but no precipitation), to obtain an initial fluid composition for the heat exchanger model. The heat exchanger is a tube model with a variable heat flux to ensure the desired temperature at the outlet of the heat exchanger using the solver which was previously explained. Precipitation in the heat exchanger due to cooling is modelled with PHREEQC. Precipitation of barite and celestite is modelled simultaneously and hence the minerals compete for sulphate. Note that this behavior would be affected by their kinetic parameters, which were not taken into account in the current study.

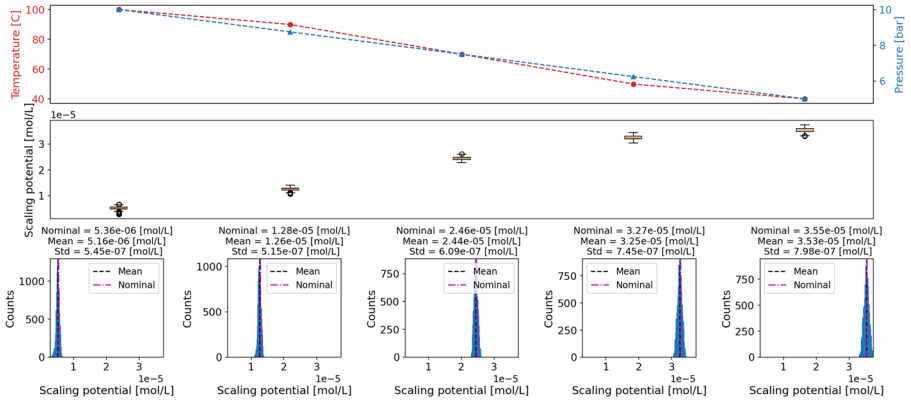

Fig. 5 Probability distribution of barite scaling potential resulting from the ~ 10,000 Monte Carlo samples of the input uncertainty at five points in the heat exchanger tube

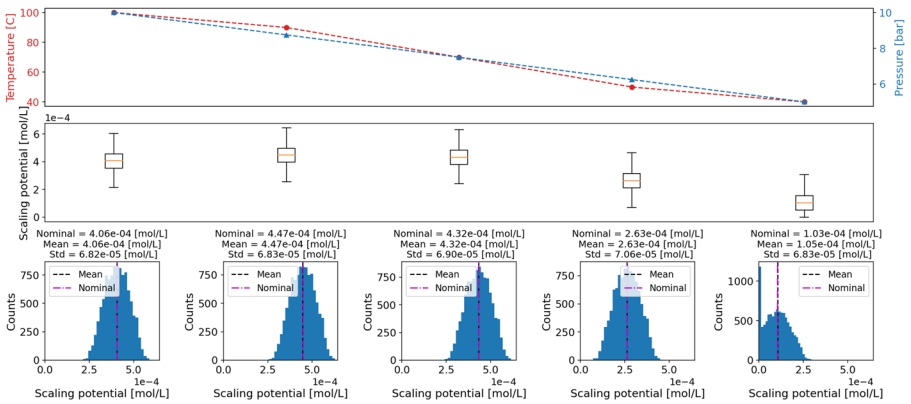

Fig. 6 Probability distribution of celestite scaling potential resulting from the ~ 10,000 Monte Carlo sample of the input uncertainty at five points in the heat exchanger tube

In the next sections, first the impact of uncertainty in brine composition on the amount of potential scaling at a given process condition is quantified with the aim of understanding which uncertain element or combination of uncertain elements has a significant impact on the scaling. Afterwards, the two-way coupled model is used to generate probabilistic forecasts of the production decline as a result of mineral precipitation under brine composition uncertainties. Finally, the optimal temperature control in the heat exchanger to maximize the coefficient of performance of the geothermal plant will be estimated using the RCP framework introduced in the previous section.

Uncertainty analysis

Figures 5 and 6 show the probability distributions of barite and celestite scaling potentials in mol/L, at different computational grid cell along a simplified heat exchanger case. For each point, roughly 10,000 samples were evaluated. The resulting barite scaling potential generally increases as the temperature decreases along the heat exchanger. On the other hand, celestite scaling potential shows a more complex relation, starting of relatively high and peaking somewhere between 90 °C and 70 °C. By comparing the probability distributions for both minerals, it can be seen that standard deviations of celestite

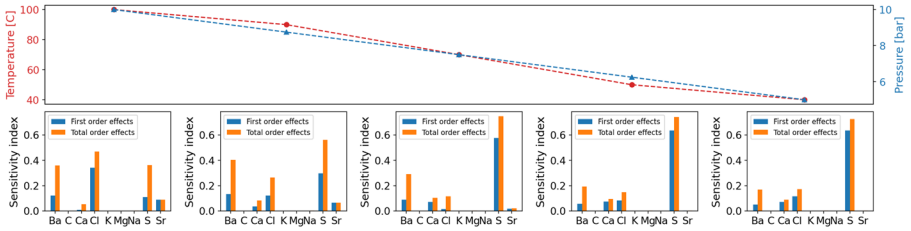

Fig. 7 First- and second-order Sobol sensitivity indices of barite scaling potential for five operating points along a simplified version of the heat exchanger case

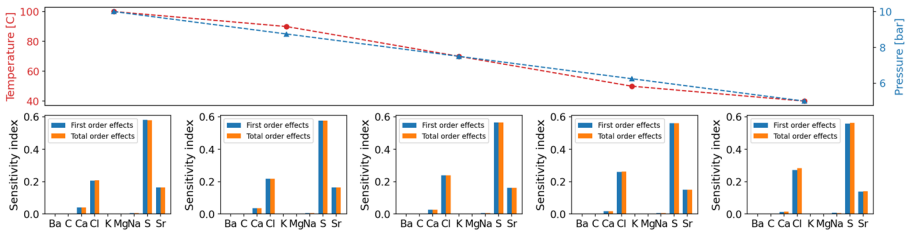

Fig. 8 First- and second-order Sobol sensitivity indices of celestite scaling potential for five operating points along a simplified version of the heat exchanger case

scaling potential are much larger, indicating that the uncertainty in brine compositions has a much larger effect on the uncertainty of celestite than that of barite. Especially the final section of the heat exchanger is expected to have large uncertainties in scaling, as here there is a chance of no celestite scaling taking place at all for a significant number of samples (over 10%). This is further exacerbated by the fact that in general the magnitude of celestite scaling is higher than barite by an order of magnitude.

To reduce the number of brine components to be considered in the subsequent UQ analyses, the Sobol sensitivity indices were determined for an initial set of nine components: sodium, potassium, carbon, calcium, magnesium, barium, chlorine, sulphur, and strontium. To ensure the Sobol indices were valid throughout the entire operating range of the modelled heat exchanger, the analysis was repeated for five computational cells along the heat exchanger tube.

Figures 8, 7 and 8 show the results of the Sobol sensitivity analysis along the heat exchanger tube for barite and celestite, respectively. There are five dominant brine elements which are impacting barite scaling potential, namely: barium, sulphur, chlorine, calcium, and strontium. Barite is a compound of barium and sulphate (BaSO4), and thus its formation primarily depends on the presence of the elements making up these two ions. In addition, both calcium and chlorine have been known to impact the precipitation chemistry of barite (Jones et al. 2004; Azaza et al. 2017; Kristensen et al. 2020). For celestite potential, four brine components are dominant, namely: calcium, chlorine, sulphur, and strontium. Apart from their relative importance, these are the same elements as those seen in the barite Sobol analysis. For celestite, no higher-order interactions between elements were found. We acknowledge that initial uncertainty perturbations applied to each elemental concentration, followed by PHREEQC adjustment of charge balance through the change of chlorine, could impact the uncertainty analysis. This process may affect the sensitivity analysis for chlorine, as the Monte Carlo sampled chlorine

concentration is not directly retained in the charge-balanced solution. Future work could explore alternative methods to address this limitation by eliminating one degree of freedom from the elemental concentrations.

Based on these results and the fact that they do not change significantly as a function of temperature and pressure, it was decided to only include barium, sulphur, chlorine, calcium, and strontium in the remaining modelling analyses. The smaller the number of components to be considered allowed the total number of Monte-Carlo samples to be decreased, reducing the computational time of the two-way coupled model for forecasting scaling and the resulting production decline.

Forecasting under uncertainty

In this section, the two-way coupled model is tested to provide a production rate forecasting impacted by the mineral precipitation in the heat exchanger under fluid composition uncertainty. For the forecasting, the impact of deposition layer growth on the flow rate reduction for a given pressure boundary condition was calculated in a time horizon of 100 days. The result of the production rate forecasting with the two-way coupled model under brine composition uncertainties is shown in Fig. 9. The results presented herein depict the decline in production and its associated uncertainties observed over a period of 100 days. The central line represents the mean of the realizations, while the box encompasses the 25th and 75th percentiles (P25 and P75, respectively) of the data distribution. In addition, the whiskers extend to denote the minimum and maximum values of all the realizations. Notably, the width of the box is not indicative of any specific parameter but is solely employed for enhanced visualization purposes. The volumetric flow rate based on the nominal concentrations for all the elements in the brine demonstrates a gradual linear decrease in time. At the production temperature of 100 °C and at the first days of forecasting, a significant drop is observed in the production rate (approximately 10% decrease). At subsequent time intervals, slightly lesser barite precipitates due to the marginal temperature increase in the outlet of the heat exchanger, linked to the reduction in the heat transfer. The red dot indicates the mean volumetric

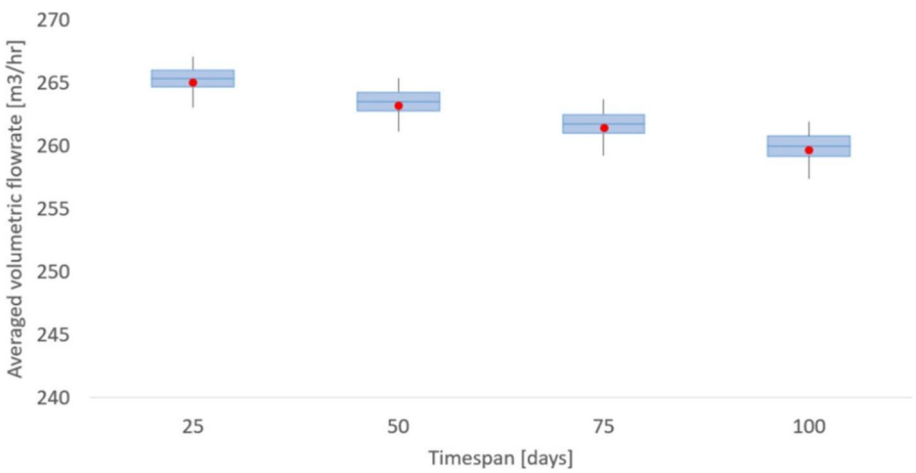

Fig. 9 Production rate forecasting under fluid composition uncertainty at the production temperature of 100 °C and a pressure drop of 5 bars

flow rate for the nominal brine composition. It is consistently lower per interval when compared with the arithmetic mean of the 100 samples. Uncertainty remains bounded by 1% higher and lower relative to the nominal composition. Consequently, an aleatoric uncertainty of 3–4% in brine concentration results in an average flow rate uncertainty of approximately 1%.

RCP results

In the case study, both barite and celestite precipitation in the heat exchanger was modelled. For RCP, only the temperature control for barite precipitation minimization is considered, since celestite is less affected. Barite precipitation can be managed by limiting the heat extraction at the heat exchanger, which, in turn, also contributes to decreasing the thermal energy produced. On the other hand, by maintaining the heat extraction from the heat exchanger at high levels, the induced precipitation in the heat exchanger creates a higher resistance in the system, and, thereby, more power is required to operate the pumps necessary for the production. In addition, uncertainty in fluid composition poses challenges to accurately predict the scaling index and amount in the heat exchanger based on the available physical models, even when the process conditions (pressures and temperatures) are known or prescribed. In this context, the goal is to optimize the plant coefficient of performance, in the presence of geochemical composition uncertainties, through the control of the outlet temperature of the heat exchanger. This requires finding the sweet spot within the operational settings that allows for maximizing thermal energy production while minimizing the precipitation and the respective incremental power consumption of the pumps. The control vector u being optimized consists of a single variable, the temperature setpoint at the outlet of the heat exchanger ($u = [T_{out}]$). The uncertainties were taken into account for the amount of barium in the brine with the considered ensemble of scenarios includes the model realizations with the original and lower barium concentrations [Ba] in the range of [0.0, 5.5] [mg/L].

Point-based optimization

Based on the first assessment of the behavior of the system, we now focus on a more refined optimization effort within the values expected to result in high COP values. The model evaluation did not reveal significant differences in terms of ideal outlet temperature across time, thus we here concentrate our attention to the COP at 100 days only. Four point-based optimization experiments have been performed to maximize COP at 100 days: three deterministic optimizations for each of the three barite concentration scenarios considered (low, nominal, high) and one scenario-based robust optimization comprising all the barite concentration scenarios simultaneously. All these experiments have been solved via exhaustive grid search for the best outlet temperature, by evaluating temperatures at every 0.1 °C.

Figure 10 depicts the optimal COP values obtained for each barite concentration scenario individually and for the ensemble of all barite scenarios considered (here assumed to be equiprobable). We observe that, despite the optimum setting being close to each other, the optimal outlet temperature values are not the same.. The optimal outlet temperature value for the ensemble is 28.2 °C, coincidentally the same as the optimum for one of the scenarios (with [Ba] = 5.5 mg/L). We also notice that some strong symmetry

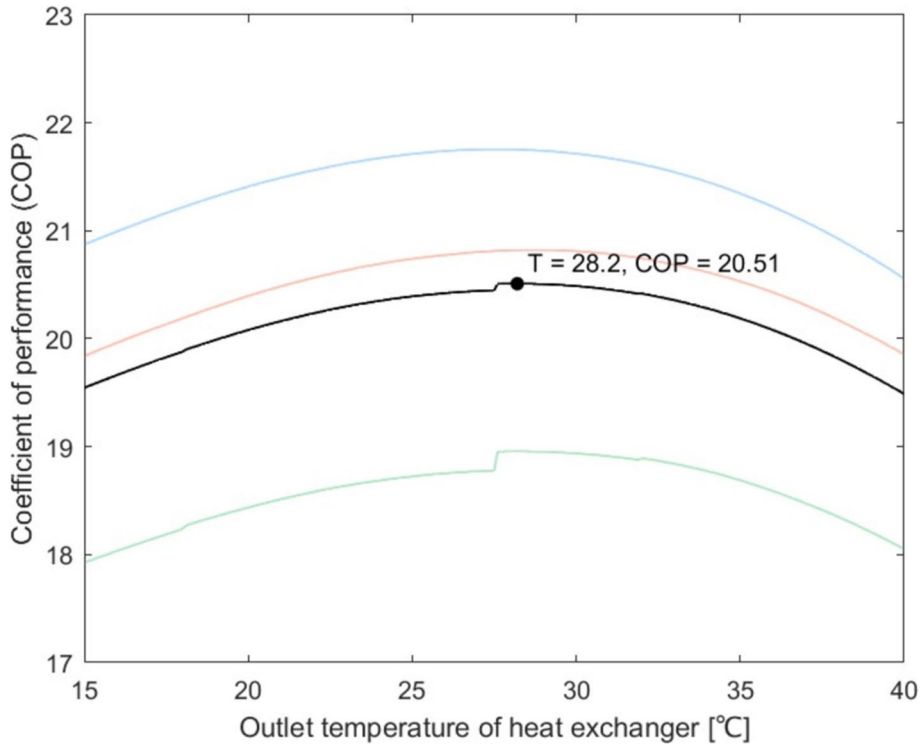

Fig. 10 Optimal COP and outlet temperatures at 100 days for the ensemble of different Ba concentrations and three lines denotes the three different Ba concentrations (low, nominal, high)

of the COP curves around the optimal outlet temperature within the inspected bounds ([15–40] °C), which has implications when searching for optimal ranges, as it will be discussed in the next section.

Range-based optimization

We investigated the range-based optimization to search for optimal ranges of outlet temperature values instead of a single most optimal value. Similar to the point-optimization problem, four optimization experiments have been performed: three deterministic optimizations for each barite concentration scenario and one optimization based on the ensemble of three scenarios, all solved via exhaustive search by evaluating temperatures at every 0.1 °C. However, in this case, each of the four experiments have been repeated for various temperature range sizes, namely, 0, 0.5, 1,... and 15 °C.

Figure 11 (left) displays the optimal COP values obtained for deterministic scenarios in the form of boxplots for two different Ba concentrations (top and bottom figures). Figure 12 (left) depicts the optimal COP values for the ensemble of scenarios in the form of violin plots to accommodate the multi-modal character of the COP distribution as a result of working with a reduced (=3) number of scenarios. These COP boxplots and violin plot show the effect of increasing the temperature range size on the COP values: while COP only drops by approximately 0.1 on average for a large temperature range size of 15 °C, the lowest COP value within the range may drop by approximately 0.4. These boxplots also exhibit a smooth quadratic trend, except for the scenario with [Ba] = 5.5 mg/L and the ensemble case due to the less symmetric behavior of the COP

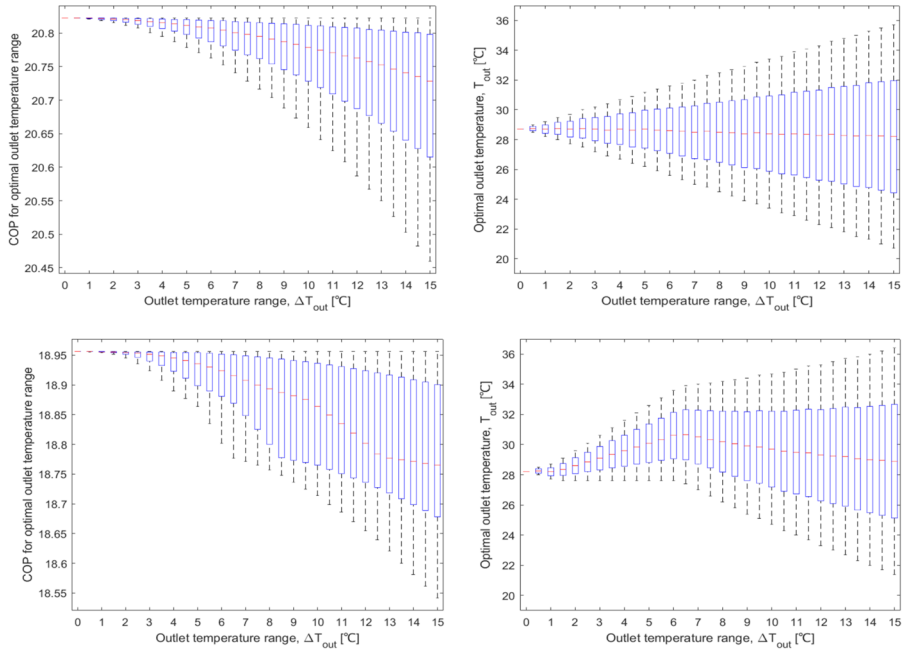

Fig. 11 Optimal range of COP values and optimal temperature ranges for two deterministic optimization based on the nominal, Ba = 2.25 mg/l (top) and high, Ba = 5.5 mg/l (bottom) concentrations. The left figures show the optimal range of COP values and the right figures show the optimal outlet temperature ranges at 100 days for varying temperature range size (0–15 °C)

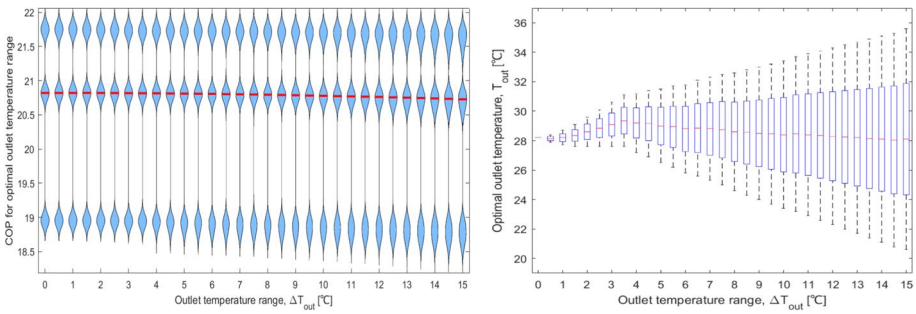

Fig. 12 Optimal range of COP values (left) and optimal outlet temperature ranges (right) at 100 days for varying temperature range sizes [0–15] °C and ensemble accounting for uncertainty on barium concentration in brine of [0–5.5] mg/L

curves seen in during point-based optimization (Fig. 10) and in which the boxplots show some deflection point around the range size of 12.5 °C (more visible in Fig. 11 left bottom). This deflection point is mainly due to a change in the precipitation regime predicted by the chemistry model around the indicated temperature. We also note that, with increasing range sizes, mainly the lowest COP value of the range decreases, while the highest COP value remains constant. This is because, in this case, all the optimal ranges do comprise the optimum of the point-based optimization.

Figures 11 and 12 (right) depict the optimal temperature ranges obtained for the respective cases. Like for the COP boxplots, the optimal temperature ranges show a fairly symmetric trend for scenarios with lower Ba concentrations, but a distinct

non-monotonic trend for the cases with the highest Ba concentrations, [Ba] = 5.5 mg/L, and the ensemble. On the other hand, while for the scenario with [Ba] = 5.5 mg/L the tipping point in the optimal temperature ranges occurs for a range size of 6 °C, for the ensemble case this appears for a range size of 4 °C. This is also the temperature range size at which the range of COP values for the ensemble case starts to drop more visibly. This suggests that operating the system within control range of 4 °C would be compatible given the degree of uncertainty on barium concentration varying between [0–5.5] mg/L. In other words, controlling outlet temperatures with more accuracy than that would not be directly beneficial unless the uncertainty on barium concentration can be resolved.

Impact of ensemble distribution

The range-based optimization results presented in previous sections were obtained through optimization over the ensemble of model realizations, considered to be equiprobable (i.e., following a uniform probability distribution). Based on previous assessments, this distribution could be different, where the scenario with [Ba] = 2.25 mg/L is more likely to occur. To investigate the impact of the ensemble probability distribution, we repeated the range-based robust optimization and analysis for a new distribution, namely, $p_1 = 0.25$, $p_2 = 0.5$ and $p_3 = 0.25$. This means that now the robust optimization optimizes the weighted average of the COP objective function and the boxplots and violin plot reflect new realization weights as well.

Figures 13 and 14 display the obtained results. While the optimum solution of the point-based optimization does not change with the new scenario probabilities,

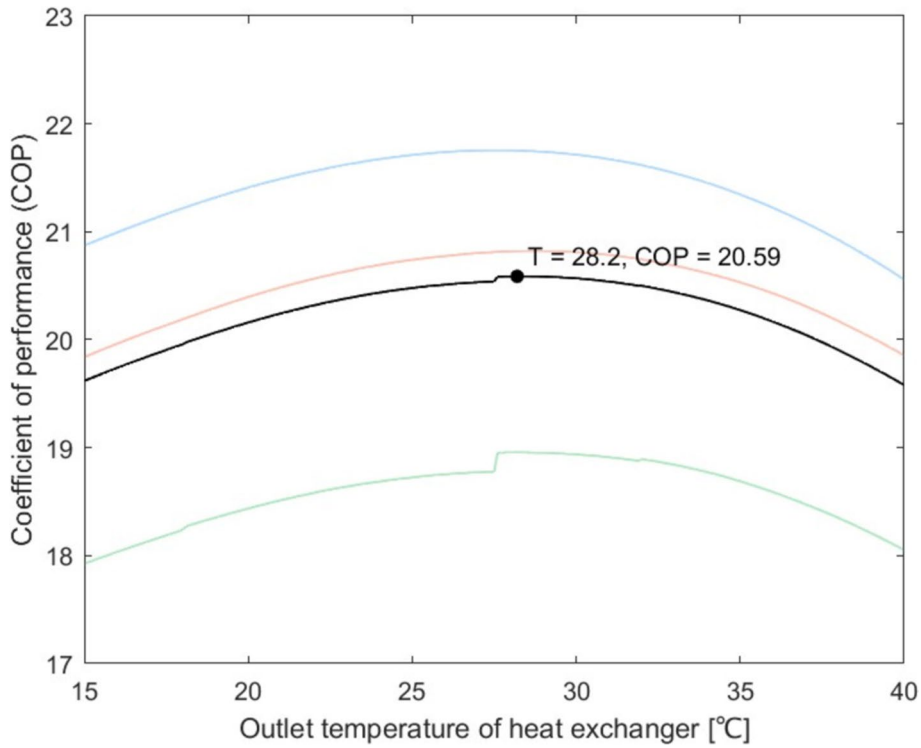

Fig. 13 Optimal COP for the ensemble of realizations using a new probability distribution

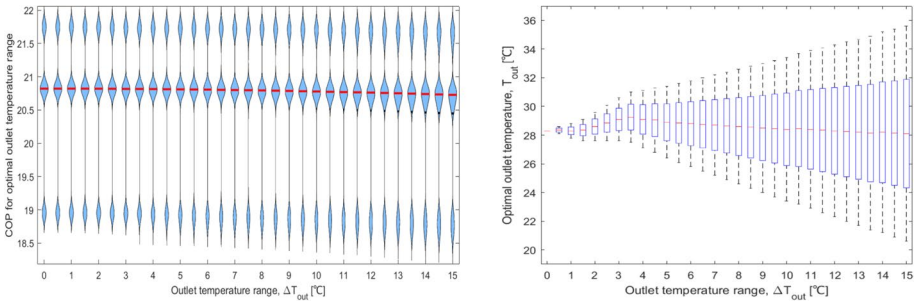

Fig. 14 Optimal range of COP values (left) and optimal outlet temperature ranges (right) at 100 days for varying temperature range sizes [0–15] °C and ensemble accounting for uncertainty on barium concentration in brine of [0–5.5] mg/L

these results do highlight the benefit of following a scenario-based robust optimization approach. A simplistic way of working with the most-probable scenario only ([Ba] = 2.25 mg/L, with p2 = 0.5) would have led to an optimum outlet temperature value of 28.7 °C [see Fig. 10 (left)], whereas the scenario-based robust approach based on the ensemble points to an optimum outlet temperature of 28.2 °C. In addition, the range-based optimization results do not change much with the new scenario probabilities. The general trend remains similar and the variability in COP values is, once more, mostly due to the uncertain scenarios rather than the temperature range sizes. The only small difference observed with respect to the previous ensemble case (with equiprobable realizations) is that the range size at which the COP distribution starts deviating more noticeably is around 3.5 °C instead of 4 °C from the previous case, which means that based on this state of probabilities 3.5 °C would be a suitable maximum accuracy to control the outlet temperatures. Despite a small change in the outlet temperature control as a result of different probability distribution, the results show the importance of having a representative and statistically significant probability distribution of the uncertain parameters. The changes in the optimal COP and outlet temperature range can be case dependent and for some production regimes or mineral precipitation, the impact of uncertainty can lead to a higher change in these values.

Summary and conclusions

An accurate prediction and robust control of the geothermal production is of great importance in the operational decision-making processes. This study introduces a structured approach for guiding operational decisions under fluid composition uncertainties. We have devised a workflow employing a scenario-based control algorithm. This algorithm aids in identifying optimal production strategies to improve the performance of geothermal systems while minimizing the adverse effects caused by scaling. For this purpose, a numerical modelling framework was developed to describe the geothermal fluid and heat transfer in the geothermal plant with brine composition uncertainties. A mechanistic 1-D fluid flow model was two-way coupled with a speciation model to estimate the potential precipitation amounts of selected minerals in a geothermal system. An additional precipitation and roughness model was developed and tested to account for the impact of precipitation on the hydrodynamic of the flow. This workflow was

combined with an uncertainty quantification method to account for the uncertainties or variations in the produced geothermal fluid composition.

The developed workflow was demonstrated in a case study of temperature control in a geothermal plant with barite and celestite precipitation. As the first step, the impact of uncertainty in the brine composition on the scaling potential was investigated by Monte-Carlo sampling. For barite, this uncertainty in water composition and related impact on scaling was found to be lower than for celestite. This change was mainly explained due to a higher concentration of strontium (a main component of celestite) than barium for the selected case study. In addition, it was found that while both compounds precipitated throughout the heat exchanger, the impact of heat transfer control (outlet temperature control) on barite was more significant. Sobol variance analyses provided information on the most significant components impacting the precipitation estimation, which for this case study there were mainly barium, sulfur, calcium, chlorine, and strontium. The forecasting of the production rates under composition uncertainties showed the confidence levels in the forecasting. In this case study, the uncertainties in the brine composition (around 2–4% uncertainties) had a relatively low impact on the uncertainties in the production rate forecasting (around 1% uncertainties).

Finally, the RCP workflow was applied on the case study to optimize the geothermal production COP through temperature control in a heat exchanger. The analyses were done for both point-based and range-based optimization. The results showed the importance of taking into account the uncertainties in the brine composition on determining the optimal conditions for the operation (in this case temperature control in a heat exchanger). For the range-based optimization, the analyses provided recommendations on the required accuracy for the outlet temperature control given a certain probability distribution for the uncertain brine component. Finally, the impact of probability distribution on the optimal temperature control was assessed, showing the importance of using a representative distribution function for the uncertain parameters. For the current case study, a change of 0.5 °C in the optimal outlet temperature range was found which translates into 12.5% change as a result of probability distribution variations. All the observations and conclusions from the case study depend on the selected models, methods to handle uncertainties, uncertain parameters, and range of uncertainties and hence no specific or generalizable conclusions can be drawn regarding the details of the case study.

The generic workflow to account for uncertainties in the modelling and optimization has several applications for the design and operation of geothermal plants. In case of other types of scaling in which several parameters will impact the scaling in different locations, e.g., calcite precipitation, it will be necessary to control both pressure and temperature across the plant. In addition, other parameters can act as inhibitors, such as CO_2 dosing and pH control. In this scenario, we need to optimize the plant by controlling pressure, CO_2 dosing and inhibitor dosage (e.g., HCl) and we have as control variables $u = [p, CO_2, HCl]$, at each time t, and the uncertainty is the composition of minerals and gas in the brine, $w = [c, g]$. The workflow can be used to control the injection and production rates to account for other production issues, such as corrosion, erosion, and pump failures. For the design aspects, the efficiency and design of ion exchange filters under brine composition can also be estimated using the current workflow.

Another important perspective topic is the extension of the uncertainty quantification framework to include epistemic uncertainties associated with the choice of thermodynamic databases and models. This will involve exploring multiple thermodynamic databases to account for variations in activity models, mineral solubility constants, and their dependencies on pressure and temperature. By systematically accounting for these sources of epistemic uncertainty, the impact of database selection on model predictions can be quantified using experimental data. This approach will complement the current assessment of aleatoric uncertainty and provide a more comprehensive understanding of the system's behavior under uncertainty.

Acknowledgements
This study was performed as a part of REFLECT project which has received funding from the European Union's Horizon 2020 research and innovation program under grant agreement n° 850626.

Author contributions
P.S.O. developed the full framework, collected the data and developed the case study, conducted the modelling and uncertainty propagation activities, wrote the main manuscript. J.P. and P.S.O. performed the UQ and Sobol analysis. E.B., C.G.M. and P.S.O have supported the optimization problem formulation and thoroughly analyzed the outcome of the optimization problem. H.Z. developed the roughness model. L.W. supported the geochemistry base model and consulted us with the uncertainties in the brine composition. A.T. supervised the flow modelling developments. H. R. and S.S.T have critically reviewed the assumptions and approach for the modelling and optimization. All authors have contributed to the writing and reviewing of the manuscript.

Funding
This study was performed as a part of REFLECT project which has received funding from the European Union's Horizon 2020 research and innovation program under grant agreement n° 850626.

Availability of data and materials
All data anlaysed in this study are presented in the manuscript. The data used for fluid properties is retrieved from REFLECT database which is accessible via the website and fluid atlas: REFLECT H2020 Project (reflect-h2020.eu). Specific data concerning the case study can be made available upon request. An example of the uncertainty quantification workflow connected to PHREEQC model is accessible via: GitHub—poortjp/REFLECT_D4-3_example: Example of MATLAB script for automated uncertainty quantification sample generation an calculation of geothermal scaling.

Declarations

Ethics approval and consent to participate
Not applicable.

Consent for publication
Not applicable.

Competing interests
The authors declare no competing interests.

Received: 13 June 2024 Accepted: 17 January 2025
Published online: 27 January 2025

References

Andre L, Christov C, Lassin A, Azaroual M. A thermodynamic model for solution behavior and solid-liquid equilibrium in Na-K-Mg-Ca-Al(III)-Fe(III)-Cr(III)-Cl-H2O system from low to very high concentration at 25 °C. Acta Sci Nat. 2019;6(1):26–36.

Ármannsson H, Ólafsson M. Geothermal sampling and analysis. Presented at Short Course II on Surface Exploration for Geothermal Resources, organized by UNU-GTP and KenGen, Lake Naivasha, Kenya, 2007.

Azaza H, Mechi L, Doggaz A, Optasanu V, Tlili M, Amor MB. Calcite and barite precipitation in CaCO3-BaSO4-NaCl and BaSO4-NaCl-CaCl2 aqueous systems: kinetic and microstructural study. Arab J Geosci. 2017. https://doi.org/10.1007/s12517-017-3005-1.

Bellout MC, Echeverría Ciaurri D, Durlofsky LJ, Foss B, Kleppe J. Joint optimization of oil well placement and controls. Comput Geosci. 2012;16:1061–79. https://doi.org/10.1007/s10596-012-9303-5.

Boersma A, Fischer H, Vercauteren F, Pizzocolo F. Scaling assessment, inhibition and monitoring of geothermal wells. Stanford: Geothermal reservoir engineering; 2018.

Bozau E, Häußler S, van Berk W. Hydrogeochemical modelling of corrosion effects and barite scaling in deep geothermal wells of the North German Basin using PHREEQC and PHAST. Geothermics. 2015;53:540–7.

Christov C, Zhang M, Talman S, Reardon E, Yang T. Review of issues associated with evaluation of Pitzer interaction parameters. Mineral Mag. 2012;76(6):1578.
Dwight RP, Desmedt SGL, Omrani PS. Sobol indices for dimension Adaptivity in sparse grids. Springer; 2016.
Echeverría Ciaurri D, Mukerji T, Durlofsky LJ. Derivative-free optimization for oil field operations. Comput Opt Appl Eng Indust. 2011. https://doi.org/10.1007/978-3-642-20986-4_2.
Fonseca M, Chen B, Jansen JD, Reynolds A. A stochastic simplex approximate gradient (StoSAG) for optimization under uncertainty. Int J Numer Meth Eng. 2017;109(13):1756–76.
Gnielinski V. Neue Gleichungen für den Wärme- und den Stoffübergang in turbulent durchströmten Rohren und Kanälen. Forsch Ing-Wes. 1975;41(1):8–16. https://doi.org/10.1007/BF02559682.S2CID124105274.
Grassinani M. Siliceous scaling aspects of geothermal power generation using binary cycle heat recovery. In World Geothermal Congress, Kyushu—Tohoku. 2000; 3167-3171.
Herman J, Usher W. SALib: An open-source python library for sensitivity analysis. J Open Sour Software. 2017. https://doi.org/10.21105/joss.00097.
Hörbrand T, Baumann T, Moog HC. Validation of hydrogeochemical databases for problems in deep geothermal energy. Geotherm Energy. 2018. https://doi.org/10.1186/s40517-018-0106-3.
Iwanaga T, Usher W, Herman J. Toward SALib 2.0: advancing the accessibility and interpretability of global sensitivity analyses. Socio-Environ Syst Modell. 2022;4:18155.
Jones F, Oliviera A, Parkinson G, Rohl A, Upson T. The effect of calcium ions on the precipitation of barium sulphate 1: calcium ions in the absence of organic additives. J Cryst Growth. 2004;262:572–80. https://doi.org/10.1016/j.jcrysgro.2003.10.069.
Kieling K, Regenspurg S, André L, Boeije C, Clark D, Demir MM, Eichinger F, Junier P, Kilpatrick AD, Kovács K, Mouchot J, Shoeibi Omrani P, Pluymakers A, Sanchez Miravalles A, Sigurðardóttir ÁK, Viig SO, Wasch L. The H2020 project REFLECT - Redefining fluid properties at extreme conditions to optimize future geothermal energy extraction. 2023. Eur Geol. https://doi.org/10.5281/zenodo.7882949.
Kristensen L, Dideriksen K, Holmslykke HD, Kjøller C, Larsen U, Mathiesen T, Dijkstra H, Poort J, Wasch L, Omrani PS, Regenspurg S. PERFORM WP1: Learn and Understand. Geothermica. 2020.
Kudela H. Hydraulic losses in pipes. Denver: Fluid Mechanics; 2009.
Ledésert BA, Hébert RL, Mouchot J, Bosia C, Ravier G, Seibel O, Dalmais É, Ledésert M, Trullenque G, Sengelen X, Genter A. Scaling in a geothermal heat exchanger at soultz-sous-forêts (Upper Rhine Graben, France): a XRD and SEM-EDS characterization of sulfide precipitates. Geosciences. 2021;11(7):271.
Mariotti A, Salvetti MV, Omrani PS, Witteveen JAS. Stochastic analysis of the impact of freestream conditions on the aerodynamics of a rectangular 5: 1 cylinder. Comput Fluids. 2016;100(136):170–92.
Moriconi L, Nascimento T, de Souza BGB, Loureiro JBR. Top-down model of calcium carbonate scale formation in turbulent pipe flows. Thermal Sci Eng Progress. 2022;28: 101141.
Parkhurst DL, Appelo CAJ. User's Guide to PHREEQC (Version 2)—a computer program for speciation, batch reaction, one-dimensional transport, and inverse geochemical calculations. US Geological Survey Water-Resources Investigations. 1999.
Pauwels J, Salah S, Vasile M, Laenen B, Cappuyns V. Testing the stability of chemical inhibitors at geothermal conditions and their efficiency to prevent galena formation. Geothermics. 2022;102:102380.
Pitzer K. Thermodynamics of electrolytes. I. Theoretical basis and general equations. J Phys Chem. 1973;77(2):268–77.
Pitzer K. In activity coefficients in electrolyte solutions. 2nd ed. Boca Ration: CRC Press; 1991.
Poort J, de Zwart H, Wasch L, Shoeibi Omrani P. REFLECT: D4.3 impact of geochemical uncertainties on fluid production and scaling prediction. 2022.
Ramsak P. Operational issues in geothermal energy in Europe. Geothermal ERA-NET. 2015;249.
Raos S, Hranić J, Rajšl I, Bär K. An extended methodology for multi-criteria decision-making process focused on enhanced geothermal systems. Energy Convers Manag. 2022;258:115253.
Regenspurg S, Feldbusch E, Byrne J, Deon F, Driba DL, Henninges J, Kappler A. Mineral precipitation during production of geothermal fluid from a Permian Rotliegend reservoir. Geothermics. 2015;54:122–35. https://doi.org/10.1016/j.geothermics.2015.01.003.
Saltelli A, Annoni P, Azzini I, Campolongo F, Ratto M, Tarantola S. Variance based sensitivity analysis of model output. Design and estimator for the total sensitivity index. Comput Phys Commun. 2010;181(2):259–70. https://doi.org/10.1016/j.cpc.2009.09.018.
Shabani A, Sisakhti H, Sheikhi S, Barzegar F. A reactive transport approach for modeling scale formation and deposition in water injection wells. J Petrol Sci Eng. 2020;190: 107031.
van den Heuvel DB, Gunnlaugsson E, Gunnarsson I, Stawski TM, Peacock CL, Benning LG. Understanding amorphous silica scaling under well-constrained conditions inside geothermal pipelines. Geothermics. 2018;76:231–41. https://doi.org/10.1016/j.geothermics.2018.07.006.
Wasch L, Shoeibi Omrani P, Twerda A. Integrated scale management for geothermal. In Proceedings of the European Geothermal Congress. 2019;6
Willmott C, Kenji M. On the use of dimensioned measures of error to evaluate the performance of spatial interpolators. Int J Geograph Inform Sci. 2006. https://doi.org/10.1080/13658810500286976.
Zhang J. Modern Monte Carlo methods for efficient uncertainty quantification and propagation. Wiley Interdiscip Rev Comput Stat. 2020;13:1539.

Publisher's Note